applied sciences

MDPI

Article

Development and Evaluation of Customized Bike Saddle Pads Using Innovative Design for AM Approaches and Suitable Additive Manufacturing Processes

Sebastian Geyer [1,2,*], Jonas Schwemmer [2] and Christian Hölzl [3]

[1] Institute of Material Science and Technology, Faculty of Mechanical and Industrial Engineering, TU Wien, Getreidemarkt 9, 1060 Wien, Austria
[2] High Tech Manufacturing, Department of Engineering, University of Applied Sciences, FH Campus Wien, Favoritenstraße 226, 1100 Wien, Austria; jonas.schwemmer@stud.fh-campuswien.ac.at
[3] Civil Engineering and Construction Management, Department of Building and Design, University of Applied Sciences, FH Campus Wien, Favoritenstraße 226, 1100 Wien, Austria; christian.hoelzl@fh-campuswien.ac.at
* Correspondence: sebastian.geyer@fh-campuswien.ac.at; Tel.: +43-1-606-68-77-2313

Abstract: Design for additive manufacturing (DfAM) has made significant advancements in recent years, with development focusing on pivotal aspects such as topology optimization (TO), generative design (GD), lattice structures, and AI-based algorithms. This paper puts forth a proposed methodology for the development of customizable bike saddle pads for manufacturing with AM. The approach entails the selection of appropriate AM processes and materials, the evaluation of material properties through compression testing, an initial saddle pressure mapping and bike fitting, the design and AM of bespoke saddle pads based on the initial measurements, and a validation pressure mapping and bike fitting. The investigation yielded clear findings regarding improvements in both pressure distribution and the change in pressure peaks, as well as an improvement in riding comfort. The findings indicate that although the overall process is innovative, improvements are required to streamline the measuring, modeling, and manufacturing workflow.

Keywords: additive manufacturing (AM); design for additive manufacturing (DfAM); lattice structures; CAD; road bike saddle

Academic Editors: Manoj Gupta, Sangjin Jung and Giangiacomo Minak

Received: 5 November 2024
Revised: 23 December 2024
Accepted: 3 January 2025
Published: 6 January 2025

Citation: Geyer, S.; Schwemmer, J.; Hölzl, C. Development and Evaluation of Customized Bike Saddle Pads Using Innovative Design for AM Approaches and Suitable Additive Manufacturing Processes. *Appl. Sci.* **2025**, *15*, 472. https://doi.org/10.3390/app15010472

1. Introduction

Additive manufacturing (AM), also known as 3D printing, is considered one of the most innovative manufacturing technologies of the 21st century and has gained increasing importance in industrial applications in recent years due to significant benefits such as saving raw materials, increased design freedom and freedom of form, and reduced cycle times [1,2]. AM enables the creation of intricate geometrical features with ever-improving precision, obviating the necessity for cutting tools, dies, fixtures, or other intricate machining processes [3]. The emergence of AM has had a profound impact on numerous facets of contemporary life. This has resulted in a series of profound shifts, including those in society, consumerism, engineering [4], economics [5], education [6], policy [7], and healthcare [8].

AM processes such as vat photopolymerization (VPP), powder bed fusion (PBF), and material extrusion (MEX) are amongst the most commonly utilized for the fabrication of components within the industry [9]. According to Wohlers Report 2023, the PBF of polymers (e.g., SLS, MJF, SAF) was the leading technology in the industry and MEX the most used technology in the consumer market in 2023. The laser powder bed fusion (LPBF)

of both metals and polymers is employed in applications pertaining to the aerospace and automotive industries, and it is regarded as the most effective approach [10,11].

The implied design freedom and the freedom of form of AM are significant drivers in the development of parametric CAD solutions such as nTopology nTop [12], Altair® Sulis™ [13], Altair ® Inspire™ [14], Carbon® Design Engine Pro [15], Autodesk Netfabb Ultimate [16], and Metafold [17] currently available on the market. Design mechanisms such as topology optimization (TO), generative design (GD), and lattice structures are commonly used in conjunction with AM to reduce weight and material cost and simultaneously maximize the stiffness or flexibility of part designs.

Cellular materials are frequently encountered in nature in the form of sponge and coral structures, as well as wood and trabecular bone material. In biological systems, these structures are composed of prismatic or polyhedral networks of solid struts or plates, which serve to define the edges and faces of individual cells, thereby filling space and bridging distances [18]. Gibson and Ashby proposed that cellular structures encompass open cells, as well as closed cell foams, honeycombs, and lattice structures. However, the latter differs from honeycombs and foams in that the cell topology, scale, and properties are defined differently [19]. In the industry, cellular structures are made from metals, polymers, ceramics, or glasses [18]. The term lattice structure derives from the former more widely used term cellular structure, as it was originally proposed by refs. [20,21]. Lattice structures are currently under investigation or even employed in a multitude of industrial sectors, including aerospace [10,22], marine [23], and automotive engineering [24], as well as in the fields of medicine biomedical engineering [25] and the sports equipment industry [26].

All lattice structures, regardless of whether they are strut-based or surface-based, can be either constant or gradient and conformal or non-conformal. Their surface limit can either be straight/angled, described by a spline, or it can be defined as open.

It is essential to consider and meticulously adjust all previously mentioned variables, such as unit cell topology [27], conformity [28], progressivity [29,30], surface limitation [19], and unit cell distribution [31] (periodic or stochastic), when designing applications in order to achieve a highly functional and resilient part with distinctive properties, manufactured using functionally graded strut-based lattice structures with both open and freeform surface limits.

This contribution aims to present an innovative approach to the design of individually customized road bike saddle pads. The approach involves the use of initial pressure mapping and bike fitting to determine the optimal position and pressure distribution for each rider's anatomy, coupled with the careful selection of both AM materials and the corresponding processes. This is followed by the design of bespoke saddle pads using conformal gradient Voronoi-based lattice structures, which are then validated through a second pressure mapping and bike fitting process. The objective of the pad design is to enhance the rider's comfort during extended periods of cycling and to mitigate the risk of developing mid- and long-term issues, including discomfort in the pelvic floor muscles, soreness, fatigue, and nerve damage.

2. Materials and Methods

It was essential to determine the fundamental principles upon which the saddle pads were to be constructed in advance. In addition to the saddle pad, which was the primary focus of this study, it was essential to utilize a carbon fiber-reinforced polymer (CFRP) shell to which the saddle pad could be securely attached. This was to provide the saddle pad with the overall form and stiffness required for the endeavor. Moreover, a measurement system was required to conduct saddle pressure assessments and yield actionable insights. To this end, inquiries were made to bicycle dealers offering a service known as "bike

fitting", which includes saddle pressure measurements. Veletage Gmbh, a local bike salon, generously agreed to provide a customized measuring system consisting of a sleeve with an array of 64 pressure sensors that fits snugly over the saddle. The measuring system consisting of the sensor sleeve and the corresponding software was provided by the well-known research institute SnM gebioMized GmbH (SnM gebioMized, Münster, Germany). Bjorn Cycles (Bjorn d.o.o.) (Domžale, Slovenia), a renowned saddle manufacturer, provided eight CFRP saddle shells for use in this project.

Three test subjects of similar weight, height, and crotch length were selected for the saddle pressure measurements (Table 1), and the pressure distribution on the saddle was subsequently measured. In order to ensure the comparability of pressure measurements, it was essential to adhere to a set of criteria that could have potentially influenced the measurement outcome.

Table 1. Body height and body weight of the three test subjects.

Test Subject	A	B	C
Body size [cm]	184	180	185
Body weight [kg]	81	82	80

It was therefore of the utmost importance that the seat positions, inclusive of the parameters established on the test subjects' bicycles by means of bike fitting processes for each rider, were precisely identical for both measurements, as there is a correlation between the pressure distribution on the saddle and the rider's seat position. To achieve this, the essential measurements of each rider's bike geometry were determined using a three-dimensional measuring system based on four cameras and affixed markers on pivotal points of the test bike (Figure 1). The aforementioned measurements were instrumental in enabling the configuration of the test bike with the requisite precise measurements for all three test subjects at each measuring event.

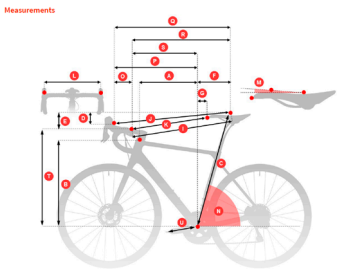

(**a**)

BIKE FRAME & CRANKSET		**HANDLEBAR**	
N Effective seat tube angle	**71 deg.**	R Handlebar Reach (from saddle)	**686 mm**
A Frame Reach	**354 mm**	E Handlebar Drop	**61 mm**
B Frame Stack	**535 mm**	K Handlebar Reach (direct from saddle tip)	**551 mm**
U Crank Length	**L: 172.5 mm**	S Handlebar Reach (from BB)	**462 mm**
	R: 172.5 mm	T Handlebar Stack (from BB)	**619 mm**
SADDLE		**GRIP**	
C Saddle Height	**720 mm**	L Grip / Handlebar Width	**419 mm**
G Saddle Set Back	**84 mm**	P Grip Reach (from BB)	**551 mm**
F Saddle BRP Set Back	**223 mm**	Q Grip Reach (from saddle)	**774 mm**
M Saddle Angle (positive = tilted upwards)	**1 deg.**	J Grip Reach (direct from saddle center)	**806 mm**
H Max. pedal to saddle BRP distance (C+crank)	**893 mm**	D Grip Drop	**67 mm**
I Saddle BRP to stem direct distance	**689 mm**	O Grip Reach (from handlebar)	**88 mm**

(**b**)

Figure 1. Essential bike geometry measurements determined for test subject B during the initial bike fitting process; (**a**) visual representation and (**b**) corresponding measurements.

The utilization of road bike shoes with a clipless pedal system was employed to prevent the shoe position from slipping during the bike fitting process. Each test subject was permitted to select their own cycling attire according to personal preference. It is important to note that the selection of appropriate clothing, particularly the choice of cycling shorts, can influence the pressure distribution on the saddle. To ensure comparability between the measurements, the clothing worn by the test subjects for the first and second saddle pressure measurements was identical.

It was imperative that the saddle geometries utilized remain constant throughout the pressure measurements. Each test subject was provided with the same saddle geometry. The second measurement differed from the first in that all test subjects' saddles were now equipped with a bespoke saddle pad. It was challenging to ascertain the requisite

stiffness of the saddle, as each individual's subjective perception of saddle firmness differs. For purposes of comparison, the saddle with the non-personalized saddle pad (Bjorn Setka) provided by Bjorn Cycles was used at the outset, and the saddle pads designed, manufactured, and tested over the course of this study had an overall stiffness similar to that of the non-personalized saddle pad.

Saddle pressure measurements were conducted on two separate occasions. The initial data collection phase was utilized to obtain measurement data, which served as the foundation for the subsequent saddle pad lattice structure design. The aforementioned measurements were conducted on the unadorned CFRP saddle shells, which were procured from Bjorn Cycles.

In order to identify the most suitable strut thicknesses for manufacturing the saddle pads, the material identified as most suitable for the endeavor was subjected to compression testing on predefined test geometries. Following the initial pressure measurements, the data were subjected to filtering, processing, and projection onto a digital twin of the original CFRP saddle shell. Used for a similar purpose as in ref. [32], preselected Carbon® Design Engine Pro [15] was chosen and a lattice structure was designed, based on a Voronoi formulation, to fill the geometry of the virtual saddle pad. Subsequently the bespoke saddle pads for each test were manufactured via the SLS process using a Formiga P110 from EOS GmbH (Krailling, Germany).

The second measuring event was utilized to ascertain the efficacy and pressure distribution of the saddle pads, which have been designed and manufactured in accordance with pressure measurement data of the initial measurement and bike fitting event. Prior to the commencement of the second test phase, each CFRP saddle shell was equipped with a bespoke saddle pad comprising lattice structures. The test was conducted in a manner consistent with that employed in the initial saddle pressure measurement. The objective was to enhance the pressure distribution and reduce peak pressure values, both in comparison to the unmodified CFRP shells and in comparison to the existing non-personalized saddle pad produced via AM and provided by Bjorn Cycles.

3. Results

The next sections delineate the methodologies for identifying and securing the requisite assets, including the testing and validation of the predefined AM material, the initial saddle pressure measurement, the design of the actual saddle pads, suitable base cell topologies and corresponding strut thicknesses, as well as the manufacturing and validation of the ready-to-use bespoke saddle pads. Additionally, the sections discuss the implications and limitations of the respective saddle pad design.

3.1. Prerequisites

In order to successfully undertake the task of designing, manufacturing, and validating a bike saddle pad for an existing CFRP shell, it was essential to first identify and secure all necessary resources. These include the availability of AM machines and suitable AM materials at the University of Applied Sciences, the testing setup of both material and saddle pressure, suitable software tools for processing measurement data and designing the actual saddle pad, a validation testing setup, and test subjects.

3.1.1. Material and Manufacturing Process Selection

The University of Applied Sciences has many different AM processes at its disposal. However, due to the geometrical challenges inherent to intricate lattice structures, only a select few of these AM technologies were considered. One of the available PBF processes was SLS (selective laser sintering). Hot Lithographywas selected as an available and

suitable VPP technology. In addition to the preselected AM processes, suitable materials are of equal importance.

One potential material for the saddle pads under consideration was thermoplastic polyurethane (TPU). In addition to the material itself, the manufacturer of the SLS machine, EOS GmbH, provided comprehensive instructions for its utilization in production, which are elucidated in Section 3.1.2. In addition to exhibiting favorable tribological properties, the manufacturer asserts that the material exhibits high hydrolysis resistance, high UV stability, good shock absorption, and high durability, rendering the material suitable for applications that include shoe soles and lifestyle products that necessitate elastomeric properties. Furthermore, applications that are typically composed of foam can be replaced with lattice structures fabricated from EOS TPU 1301 [33]. The Shore hardness of the material is indicated as 87A. The default color of the material is white.

Another noteworthy material for the fabrication of the developed saddle pads is Evonik's Infinam® FL 6300 L powered by Cubicure [34]. This material can be processed in Cubicure's machines, such as the Caligma [35]. These machines, one of which is located in the AM lab at the University of Applied Sciences Vienna, are based on the Hot Lithography process [36]. Evonik Infinam® FL 6300 L is defined as a rubber-like material that can be used in a variety of applications, including seals, handles, and dampers. Additionally, the material is purported to be suitable for utilization in all domains of AM, spanning from the creation of prototypes to the manufacturing of industrial series. Another noteworthy attribute of the material is its low-temperature elasticity. The default color is purple.

Following a comprehensive evaluation of both the SLS and Hot Lithography processes, it was determined that the SLS method would be utilized for the fabrication of the bespoke saddle pads. This outcome can be attributed to the advantageous material properties of the TPU material in comparison to the Infinam material. The TPU material exhibited a significantly higher Young's modulus and elongation at break, resulting in components that are more robust and durable. Furthermore, the powder-like texture of the TPU material on the saddle pads offers enhanced friction, thereby ensuring a more stable position on the saddle compared to the smoother surfaces achieved by the Hot Lithography process, where sliding is more prevalent. This consideration assumes particular significance in the case of bespoke saddle pads, given the relatively limited margin for error in assuming optimal positioning on the saddle by the rider.

The selected unit cell size for both the compression test specimens and the saddle pads was chosen as 7 mm in all principal directions. This is due to the fact that the use of smaller cells has been found to cause issues during the production process (see also Sections 3.1.2 and 3.5), while larger cells have an adverse effect on the resolution of the structure, making it challenging to accurately capture the desired saddle geometry. These observations have been made following an analysis of a series of test prints with varying cell size and strut thicknesses.

3.1.2. Compression Testing

In order to ascertain the impact of strut thickness on lattice stiffness in the selected TPU material, compression tests were conducted on predefined test specimens. Cylindrical parts interspersed with Voronoi-based lattice structures with a unit cell size of 7 mm, a height of 10 mm, and a diameter of 30 mm were fabricated from the TPU 1301 material. The selected height pertains to the height of the saddle pad to be manufactured. Furthermore, a continuous bottom surface with openings on the underside of the samples, with a thickness of 1 mm, has been incorporated to facilitate the closest possible approximation to the structure of the planned saddle pad. The thickness of the struts varied between the samples, with measurements selected in 0.1 mm increments between 0.8 mm and 1.7 mm, resulting in a total of 10 test specimens. The geometry of the samples was generated with the software

Carbon® Design Engine Pro and is precisely identical between the specimens with the sole variable being the thickness of the struts. A selection of test specimens can be observed in Figure 2a. A PA12 specimen holder was employed as a solid component to guarantee that the specimens were positioned securely (Figure 2b). This ensured that the specimens could be positioned correctly and efficiently after each measurement.

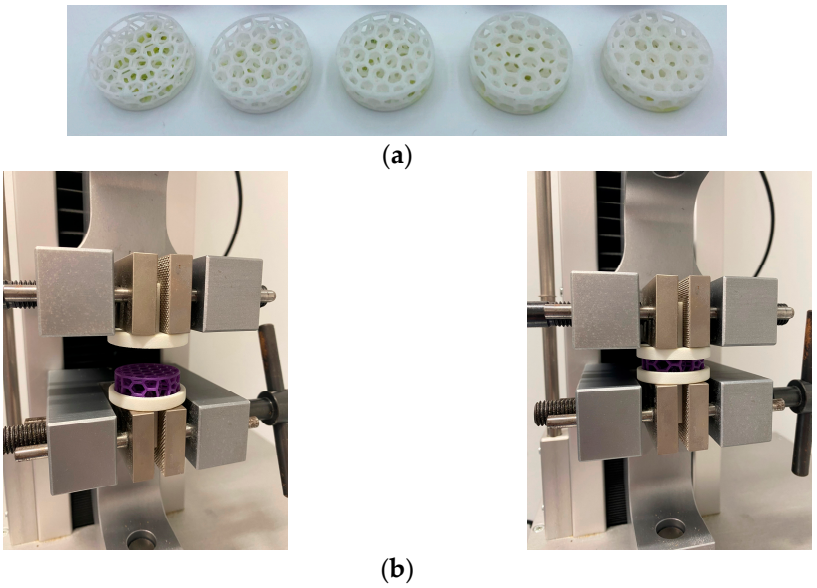

Figure 2. Test specimens and compression testing setup; (**a**) test specimens from TPU 1301, (**b**) compression test setup with AM sample holder and prepared test specimen (left), starting position (right).

Samples with a strut thickness of 0.8 to 1.3 mm exhibited a readily compressible nature when subjected to manual compression between two fingers. Manual compression was no longer a viable option for all samples with a strut thickness of 1.5 mm or greater. In purely visual terms, it was evident that as the strut thickness increases, areas that should have been devoid of material were partially filled with solidified material. This indicated that the stiffness of these components would be further augmented through the manufacturing process alone. The observed accumulation of material is presumably attributable to two factors, namely the increased use of heat during SLS, which results in the production of thicker struts, and a maximized lattice density during the respective manufacturing process.

The compression tests were conducted using a Testmatic System Z5-X1200 (Nürnberg, Germany) tensile compression testing machine. The testing machine was configured with the parameters visible in Table 2. While ISO 604:2002(E) [37] was employed for orientation purposes, it is important to note that this standard is not intended for use with test specimens comprising lattice structures. However, an overview of the classification of thermoplastic compression specimens is provided. The compression test also yielded information about the behavior of the material.

Table 2. Compression test settings.

Parameter	Value
Test speed [mm/min]	10
Max. force [N]	4500
Compression [mm]	4
Test method	Compression test
Y-axis	Force [N]
X-axis	Travel [mm]

Each sample was subjected to three consecutive tests, with a compression of 4 mm in each instance. The initial two measurements served the purpose of a precycle, facilitating the elastic deformation of the sample. It has been demonstrated that these measurements exhibited a markedly higher stiffness than the third measurement. In practical applications, elastomers are subjected to vibrations and loads that reflect real-world conditions. In the event that components have not been subjected to a load for an extended period of time, their response behavior is markedly stiffer than that of components that have been continuously loaded. The subsequent analysis was conducted using solely the values obtained from the third measurement.

A force–displacement curve was plotted for each strut thickness (0.8 to 1.7 mm in 0.1 mm increments) of each material. Figure 3a provides a comprehensive illustration of the pressure measurements obtained with the samples produced. It was of paramount importance to establish a correlation between the measured values, the values obtained from the saddle pressure measurement, and the material behavior. The objective was to predict the sinking behavior of the test subject on the bike saddle in relation to the thickness of the strut and the pressure exerted. A constant sinking behavior would permit the drawing of conclusions regarding the comfort of the saddle. This was achieved by converting the force exerted by the testing apparatus into pressure via the cross-sectional area of the cylindrical samples (706.86 mm^2). The software utilized for the measurement of saddle pressure presents the obtained values in mbar.

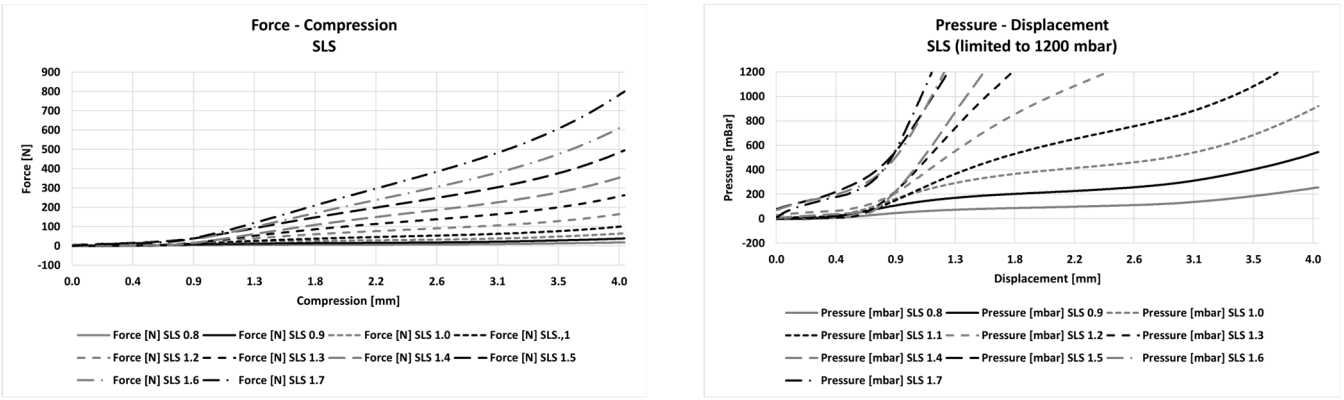

(**a**) (**b**)

Figure 3. Results of the compression tests and the force to pressure conversion; (**a**) force–compression curves, (**b**) corresponding conversions for TPU 1301, based on [38].

The maximum pressure values determined during both the initial and validation saddle pressure measurements were found to be just under 900 mbar. Accordingly, a concise illustration of the transformed pressure values in mbar is presented in Figure 3b. It can be observed that a reduction in strut thickness results in a decrease in the force required by the testing apparatus to achieve the maximum set displacement of 4 mm. Similarly, the behavior observed at the conclusion of the travel distance for strut thicknesses of 0.8 to 1.0 mm is also comparable, as can be observed in Figure 3a. It is evident that the maximum force required to achieve the maximum displacement of 4 mm increases significantly with an increase in strut thickness, particularly at 1.2 mm and above. This trend persists as the strut thickness increases further. Additionally, the distances between the maximum forces demonstrate an increase with increasing strut thickness. This indicates that the relationship between strut thickness and stiffness is not linear. However, this is to be expected, as there is no linear relationship between the hardness and stiffness of elastomeric solid parts either. Similarly, the stiffness demonstrates an exponential increase with a constant rise in hardness [37].

The increasing hardness can be considered to be equivalent to the thickness of the lattice structure. It is evident that strut thicknesses of 1.5 mm to 1.7 mm exhibit comparable behavior in this region, resulting in a similar stiffness. Thus, modifying the strut thickness on the saddle pad from 1.5 mm to 1.7 mm has no impact on the sinking behavior. In general, these strut thicknesses should be avoided, as they do not yield sufficiently with a total saddle thickness of 10 mm and also exhibit slight deformation at pressure ranges between 400 mbar and 900 mbar. The greatest scope for adjustment with regard to the possible sinking depth of the test subjects was observed between 0.9 mm and 1.2 mm strut thicknesses. It is recommended that a maximum sinking depth of 4 mm be avoided, given the potential for discomfort when the penetration depth on the saddle is also subject to significant increases in the event of vibrations. Based on the aforementioned data, a strut thickness of between 1.0 mm and 1.1 mm is deemed to be the optimal range for maximum pressure values of 900 mbar. An increase in the thickness of the struts in the areas of high pressure, up to a range of 1.3 mm, may provide the potential for additional stability.

The results of the compression tests indicated that strut thicknesses between 1.0 and 1.5 mm should be utilized for the bespoke saddle pads manufactured from EOS TPU material. The precise pressure values were derived from the initial pressure measurements of all three test subjects in Section 3.2, and the appropriate strut thickness was defined accordingly (Table 3).

Table 3. Test subject body dimensions in relation to measured peak pressures.

Test Subject	A	B	C
Body size [cm]	184	180	185
Body weight [kg]	81	82	80
Max. Pressure [mbar]	877	663	880

3.2. Initial Saddle Pressure Measurement and Bike Fitting

At the outset of the bike fitting process, the components of the test bike frame were initially aligned in a general manner according to the respective body size of the test subjects. As described in Section 2, all initial pressure measurements were performed on the unadorned CFRP saddle shell. Subsequently, the position of the hands was altered from position 1 over position 2 to position 3, and the pressure exerted on the saddle was evaluated following each transition. The aforementioned positions are elucidated in greater detail with the aid of Figure 4.

(**a**) (**b**) (**c**)

Figure 4. Riding positions and corresponding pressure measurements—blue, low pressure to red, high pressure. (**a**) Upright position 1 with the greatest pressure peaks—saddle pressure is concentrated on the rear; (**b**) standard riding position 2 with slightly bent posture, where the upper body comes further forward, thus distributing the pressure further towards the tip of the saddle; most frequently used position; (**c**) athletic position 3 with bent posture; upper body comes even further forward, thus further spreading the saddle pressure towards the saddle tip; position with the lowest pressure peaks on the saddle [39].

Once the measurement values of saddle pressure for all three hand positions had been determined, modifications were made to the settings of the test bike frame. In accordance with the test subject, modifications were made to the saddle height or the position of the cleat connection on the bicycle shoe. Subsequently, the measurement was repeated for all three handlebar positions, and the pressure on the saddle was subjected to further analysis. This process was repeated until the pressure distribution on the saddle exhibited a discernible improvement, as determined by the bike fitting expert. This was evidenced by a reduction in pressure peaks or, optimally, an even distribution of pressure (symmetry between the right and left halves of the saddle or relief of the saddle tip).

Once all measurements had been collected, the data pertaining to riding position 2 for each test subject were subjected to visualization through the use of a histogram, which demonstrated the distribution of pressure value ranges (Figure 5). The X-axis represents the various pressure ranges in mbar, while the Y-axis depicts the frequency of occurrence of these pressure values. At the outset, within the initial pressure range of 1 to 75 mbar, test subject A exhibited the highest number of measurements. While the pressure range from 76 to 501 mbar is approximately equally distributed, Figure 5a (right) shows that the range from 501 to 901 mbar is underrepresented. The pressure peak values are illustrated in Figure 5a (left). The data set as a whole indicates an unequal distribution of pressure between the two saddle halves, with the left side exhibiting higher pressure values. These peak pressure values were observed on the respective outer edges on the back of the saddle halves, as well as on the front left edge.

Test subject B exhibited the highest number of measurements in the range of 1 to 51 mbar compared to the other test subjects. With the exception of the range from 151 to 200 mbar, the pressure range from 101 to 400 mbar was approximately equally distributed, as illustrated in Figure 5b (right). As with test subject A, the data set indicates an unequal distribution of pressure between the two saddle halves, with the left side exhibiting a higher peak pressure value with 663 mbar. Additionally, a slight peak with 317 mbar is present in the saddle nose. In the range from 676 to 900 mbar, there are no pressure values present in the data set. In addition, two pressure ranges (851 to 875 and 876 to 900) are absent from the histogram, suggesting an error in the data collection.

Test subject C exhibited the highest number of measurements in the range of 1 to 50 mbar. With the exception of the range from 276 to 426 mbar, the pressure range from 151 to 551 mbar was approximately equally distributed, as illustrated in Figure 5c (right). The range from 551 to 900 mbar is underrepresented in the data set. As with test subject A and B, this data set indicates an unequal distribution of pressure between the two saddle halves, with the left side exhibiting higher pressure values. The sole exception is the absence of pressure in the saddle nose, which suggests a more uniform pressure distribution in the middle and back of the saddle. Peak pressure values were observed on the respective outer edges on the back of the saddle halves, with the left side being dominant (880 mbar) as well as on the front left edge (Figure 5c, left).

Table 3 shows the maximum pressure measured in relation to the test subject's body size and body weight. Despite the fact that all three test subjects have a similar body weight, the maximum pressure exerted by test subject B is 25% lower than that of the other two test subjects. This discrepancy may be attributed to the physical characteristics of the individual test subject.

Using the findings from both the compression testing and the initial pressure measurements, the focus of the saddle pad's development was placed on the reduction in pressure points by lowering the thickness of the struts in those areas as compared to the adjacent regions. This approach was also used in ref. [40] as opposed to the other possible approach used in the industry of stiffening the regions with high-pressure readings [41].

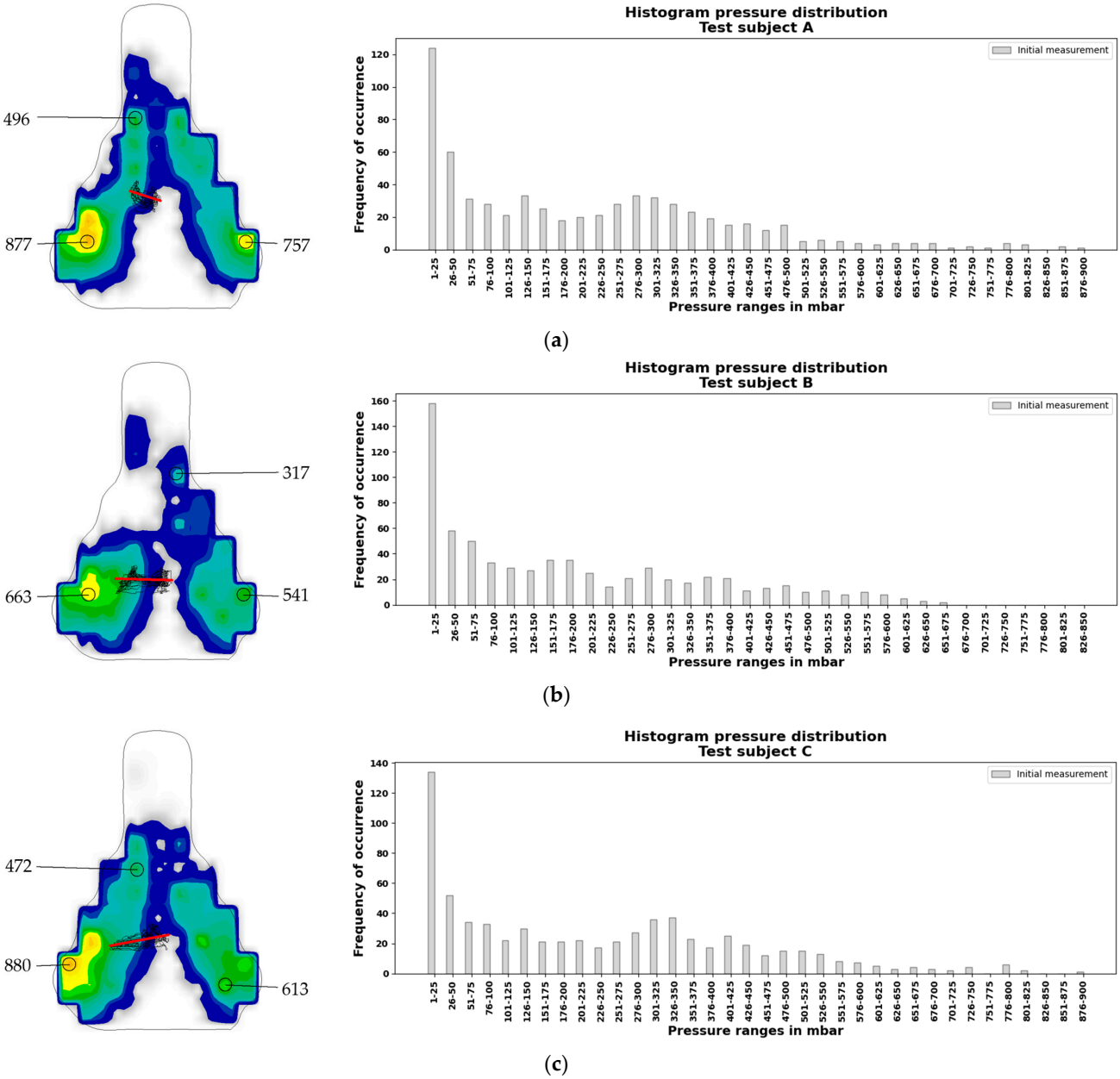

Figure 5. Visual representation of the initial pressure distribution measurements, with color plot with peak pressures on the left and corresponding histograms on the right—blue, low pressure to orange, high pressure. (**a**) Measurement of riding position 2 of test subject A, (**b**) measurement of riding position 2 of test subject B, (**c**) measurement of riding position 2 of test subject C.

Table 4 shows the defined strut thicknesses in relation to the pressure values determined in the initial pressure measurements for a Voronoi unit cell size of 7 mm. Given that test subject B exhibited a lower maximum pressure from the outset, a saddle pad version with a constant 0.05 mm lower strut thickness was produced for it.

3.3. Data Processing

Prior to undertaking the initial saddle pressure measurement, it was imperative to ascertain that the data yielded by the measurement system were of a sufficient quality to be utilized. Test data were previously made available for the examination and verification of its functionality by gebioMized. The data were presented in the form of a matrix inside a text file, in which the rows indicate the position of the pressure sensors in the X-direction and

the columns the sensor positions in the Y-direction. The actual value indicates the pressure in mbar. The provided data are available in two forms, as a real value (Figure 6a) or as interpolated values (Figure 6b).

Table 4. Defined pressure ranges with corresponding strut thicknesses derived from the initial pressure measurements.

Pressure in Mbar	Strut Thickness	
	Test Subjects A, C	Test Subject B
100	1.25	1.2
200	1.3	1.25
300	1.35	1.3
400	1.35	1.3
500	1.4	1.35
600	1.5	1.45
700	1.2	1.15
800	1.15	1.1
900	1.1	1.05

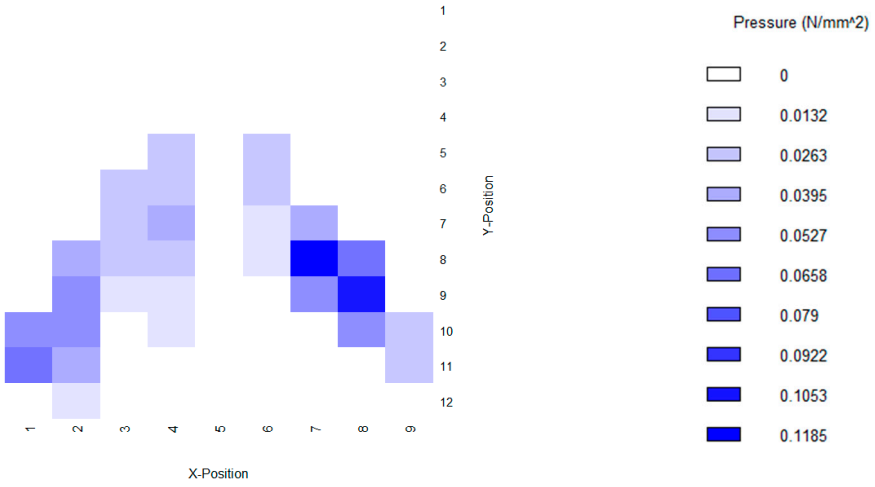

(**a**)

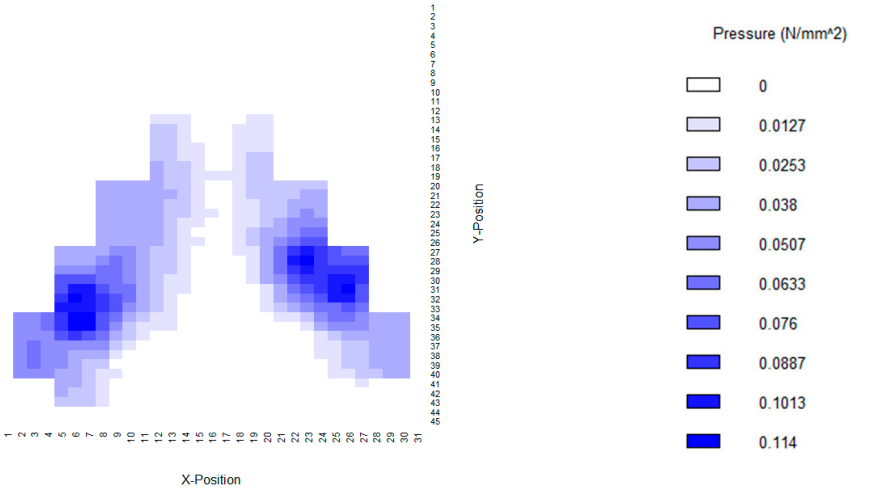

(**b**)

Figure 6. Heatmap of the provided sample raw data produced with the software R; (**a**) raw sample data set and corresponding pressure values, (**b**) interpolated sample data set with corresponding pressure values, based on [38].

The real values represent the actual measurement data obtained from the 64 pressure sensors, whereas the mathematically interpolated values provide a more detailed represen-

tation of the pressure measurement, resulting in a higher resolution. To proceed, the data had to be rendered readable for the Carbon® Design Engine Pro to generate the appropriate gradient conformal Voronoi-based lattice structure. The objective was to represent the data matrix in individual three-dimensional points and a fourth variable, which contained the pressure value at this point (X, Y, Z, pressure).

The data processing was conducted using the Rhino/Grasshopper® program (Rhino 7 SR37 (7.37.24.107.15001) Grasshopper Build 1.0.0007). An algorithm was developed in Grasshopper® to facilitate the direct generation of the final output data in a CSV MS-DOS format for the Design Engine Pro (Figure 7), based on the input matrix of the measurement system (Figure 7). The 31 × 45 (X × Y) input data matrix consisting of the interpolated values from the measuring system was employed to generate a point grid comprising X, Y, and Z variables. The X and Y values representing the coordinates of the pressure sensors were input manually into the appropriate fields. The Z value contained the saddle pressure and, as a result, did not yet represent the actual Z coordinates of the data. Subsequently, the points were projected onto the saddle surface that had been loaded in Rhino (Figure 7). Points that did not intersect the saddle surface in Grasshopper® were automatically removed by the algorithm. This permitted the generation of Z-values for the data set. In conclusion, each line of the newly generated data set comprised four values, an X, Y, and Z value (coordinates), as well as the saddle pressure at that specific point in mbar (Figure 7). The two-dimensional data set derived from the saddle pressure measurement (comprising X and Y position and pressure values at this point) was transformed into a four-dimensional data set consisting of 1.395 lines of data. After the generation of both the algorithm and the generated data set, the processed sample data were successfully tested in Carbon® Design Engine Pro.

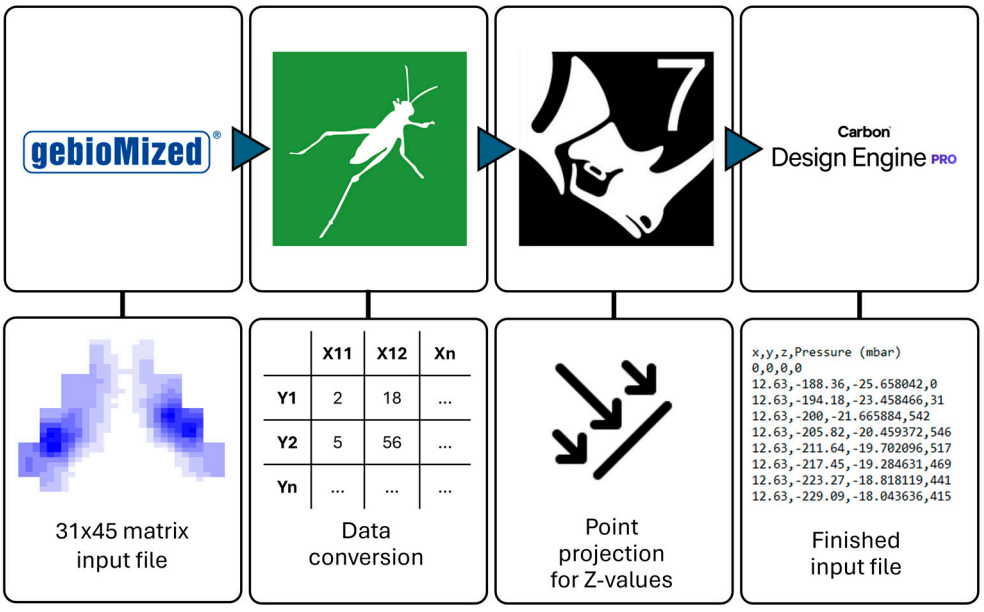

Figure 7. Data conversion workflow, interpolated data from GebioMized system is parsed into X- and Y-coordinates and corresponding pressure values using a Grasshopper® algorithm; X-Y coordinates are projected on saddle pad surface to yield Z-coordinates; finished data set is ready for input in Design Engine Pro.

3.4. Pad Design

The CAD model of the saddle pad was created by first scanning the contour of the CFRP shell using a 3D scanner and designing the base surface of the saddle pad based on the scanned data. The scanned file was imported and placed in Fusion 360. This facilitated the alignment of the splines of the 3D sketch along the contour of the shell scan (Figure 8a).

Furthermore, it was possible to place and align points on the contour in order to achieve an even more precise alignment of the surface to be created. A representation of the saddle surface structure is provided in Figure 8b.

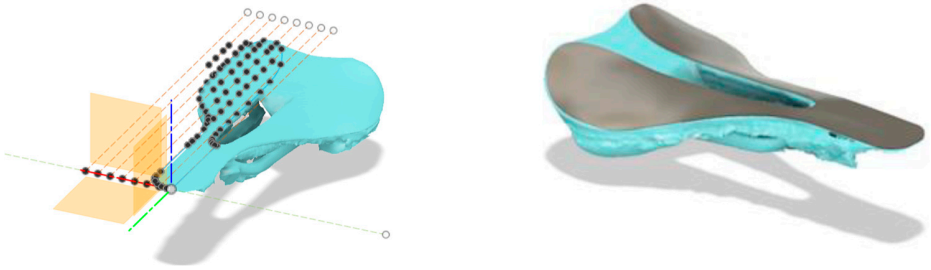

(**a**) (**b**)

Figure 8. Creation of the curved saddle surface in Fusion 360; (**a**) surface sketch on scanned STL-file and (**b**) finished surface [38].

The sketch was then thickened to the required 10 mm, the base of the saddle pad was reworked, and holes were created in the posterior region of the saddle in order to facilitate the cleaning of the printed pad from residual resin or powder material and to mitigate the risk of light or heat accumulation during the manufacturing process (Figure 9c). Furthermore, a tab was incorporated into the nose area, which can be hooked into the front part of the CFRP shell.

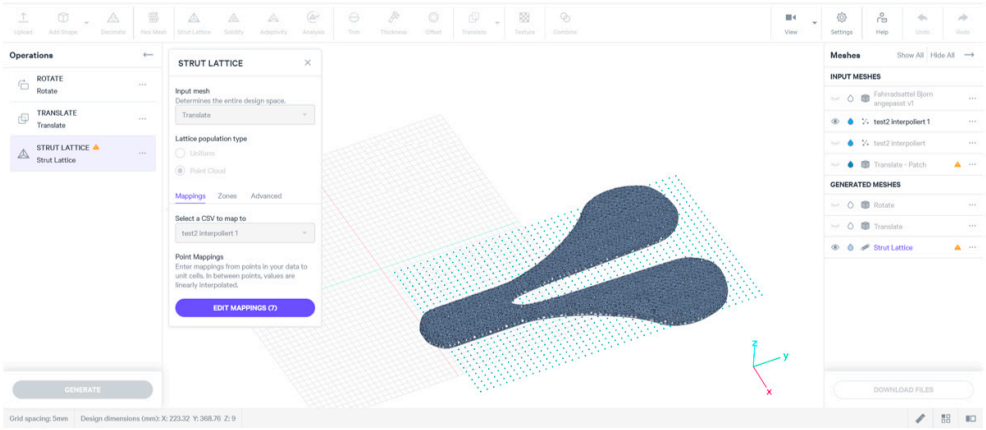

(**a**)

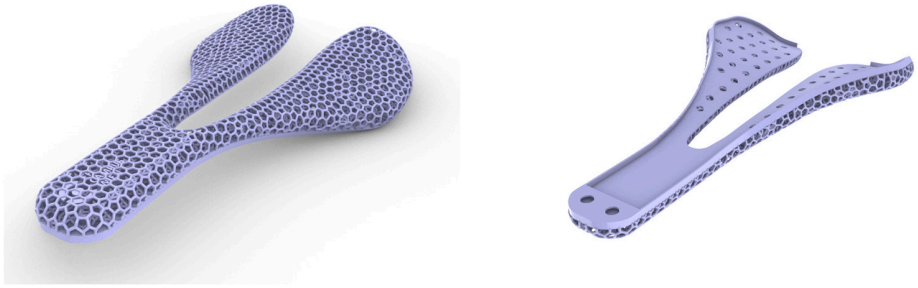

(**b**) (**c**)

Figure 9. Visual representation of the designed saddle pad; (**a**) workflow and UI in Design Engine Pro (screenshot taken: 15 March 2024), (**b**) top view of the saddle pad with gradient Voronoi lattice, and (**c**) bottom view of the saddle pad with tab in the front and holes in the back.

This prevents contact between the user and the thin CFRP shell, thereby mitigating the chafing of skin or bike shorts in this area. The completed saddle configuration was exported as a high-resolution file in Fusion 360 via the STL interface.

In Design Engine Pro, a conformal gradient lattice was constructed using the point cloud derived from the exported CSV file. In addition to the definition of the unit cell geometry as Voronoi, the strut thickness was defined according to Table 4. Defined pressure ranges with corresponding strut thicknesses derived from the initial pressure measurements and the cell size determined in Section 3.1.1 could be specified (Figure 9a). The software automatically interpolated values between the defined pressure ranges, thus assigning a corresponding strut thickness to each specific sensor value. Following the export of the CAD data from Design Engine Pro, the STL of the saddle pad was prepared for manufacturing in Magics 27. Figure 9b,c show a visual representation of the modeled saddle pad.

3.5. Pad Manufacturing

The designed saddle pads were subsequently manufactured using the selective laser sintering (SLS) process.

The design restrictions for the use of SLS necessitated, among other requirements, a minimal strut thickness of 1 mm, with the optimal range being between 1.3 and 3 mm. The dimensions of the saddle pad did not present a challenge with respect to the available build volume of 250 × 200 × 330 mm (X × Y × Z) of the machine. Accordingly, all three saddle pads were produced in a single manufacturing cycle (Figure 10a), hence demonstrating the advantage of the SLS process in terms of unnecessary support structures and the ability to stack components in a vertical configuration. Figure 10b illustrates the completed saddle pad bonded to the CFRP saddle shell, prepared for the validation pressure measurement.

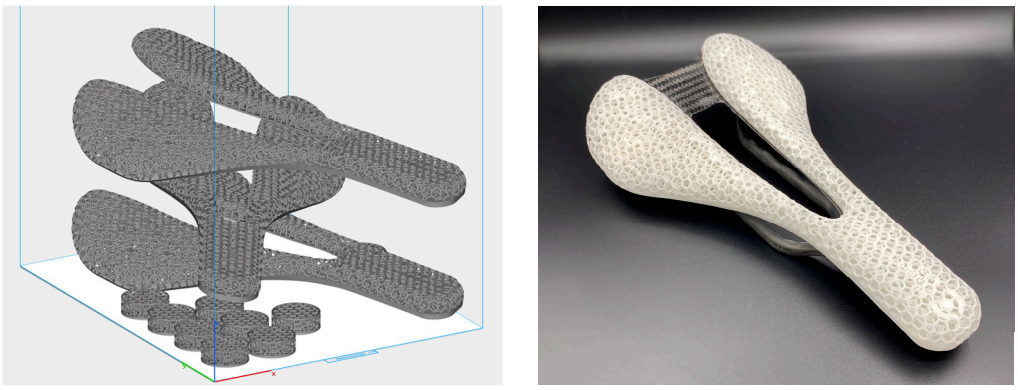

(**a**) (**b**)

Figure 10. Production of saddle pads with the SLS process; (**a**) all three pads oriented on top of each other in Materialise Magics 27 and (**b**) the finished saddle pad bonded together with the CFRP shell.

3.6. Validation Saddle Pressure Measurement and Bike Fitting

The second saddle pressure measurement was conducted in the same manner as the initial pressure measurement. The aim was to evaluate the impact of the manufactured saddle pads on the distribution of pressure across the surface of the saddle while simultaneously maintaining a stable sitting position.

A good pressure distribution image is characterized by a symmetrical and uniform shape. It is optimal that pressures above 600 mbar do not occur. However, the pressure distribution is not solely contingent on the geometry and hardness of the saddle; it is also influenced by the physical characteristics of the individual. For example, a misalignment of the hips can have a comparable impact on the pressure pattern to that of a difference in leg length or the shape of the sit bones. In cases of extreme misalignment, a personalized bike saddle can only provide a limited correction, which may not eliminate pressure peaks exceeding 600 mbar.

3.6.1. Test Subject A

The initial measurement of test subject A yielded a maximum pressure of 877 mbar in the left half of the saddle, while the right side exhibited a smaller area with a peak pressure of 757 mbar. (Figure 11a). Consequently, the pressure was higher on the left half of the saddle while simultaneously occupying a larger area. In accordance with the recommendations of the bike fitting specialist, it is likely that the left leg of subject A is somewhat shorter than the right. This discrepancy would result in increased pressure on the left half of the saddle. The lower-pressure areas were distributed symmetrically and evenly in a forward direction along the length of the saddle.

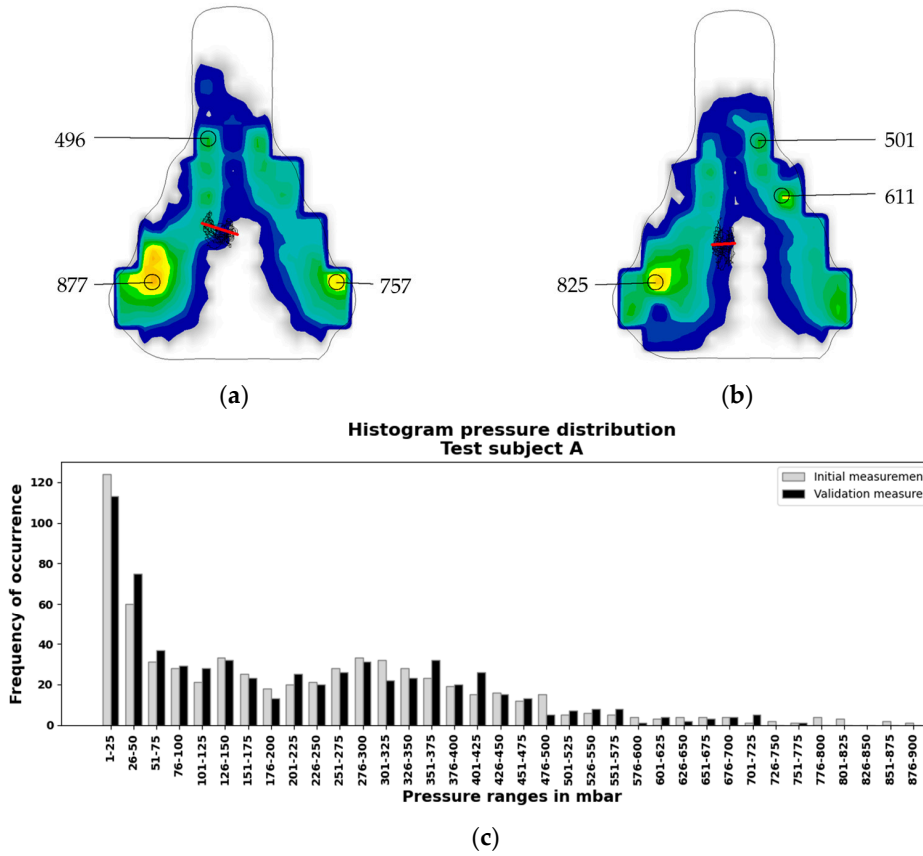

Figure 11. Visual representation of both measurements of test subject A; (**a**) color plot with peak pressure values of the initial measurement, (**b**) color plot with peak pressure values of the validation measurement – blue, low pressure to orange, high pressure, and (**c**) histogram of both measurements.

In the validation measurement, the peak pressure on the left side was reduced by approximately 15% and the right side by 17% compared to the initial measurement, as can be observed in Figure 11b. As a result of the modifications made to the area surrounding the peak pressure in order to guarantee sufficient stability, it is plausible that these areas are responsible for generating the peak pressure observed in this figure. It seems reasonable to posit that this transition (at 700 to 600 mbar) could be made even smoother, with a lower strut thickness at 600 mbar.

The histogram (Figure 11c) depicts the pressure distribution of test subject A, with the data derived from the two distinct measurements. The horizontal axis represents different pressure ranges in mbar, while the vertical axis shows the frequency of occurrence of these pressure values. Two bars are displayed for each pressure range, a gray bar for the initial measurement and a black bar for the validation measurement. At the outset, within the lowest pressure range of 1 to 75 mbar, the highest values are exhibited for both measurements. The frequency observed in the validation measurement is markedly lower

than that observed in the initial measurement. Subsequently, the frequency of the pressure values in the validation measurement increases and the validation measurement largely adheres to the frequency patterns observed in the initial measurement. It is evident that the frequencies of the validation measurement exhibit a notable increase in the ranges of 351 to 375 mbar and 401 to 425 mbar. Moreover, the maximum pressure values are observed within the maximum range of 751 to 775 mbar. In contrast, the initial measurement also demonstrated a deviation in the frequencies within the range of 876 to 900 mbar. The adapted saddle pad resulted in a slight improvement in peak pressure values for subject A. The ranges above 775 mbar are entirely absent in this instance.

3.6.2. Test Subject B

Test subject B, with a similar weight to the other two test subjects, exhibited a peak pressure that was nearly 24% lower than that of test subjects A and C in the initial measurement. Consequently, the adapted saddle pad for test subject B was manufactured with a strut thickness reduced by 0.05 mm. The pressure image shown in Figure 12a depicts the initial measurement on the CFRP shell of test subject B. It is notable that the left half of the saddle is loaded to a greater extent than the right half. Furthermore, the measurement indicates the presence of elevated pressures on the anterior aspect of the saddle, which is an unfavorable outcome in this region. As per the recommendations of the bike fitting expert, test subject B exhibits a slight pelvic tilt, which is the probable cause of the unequal peak pressure distribution on the saddle.

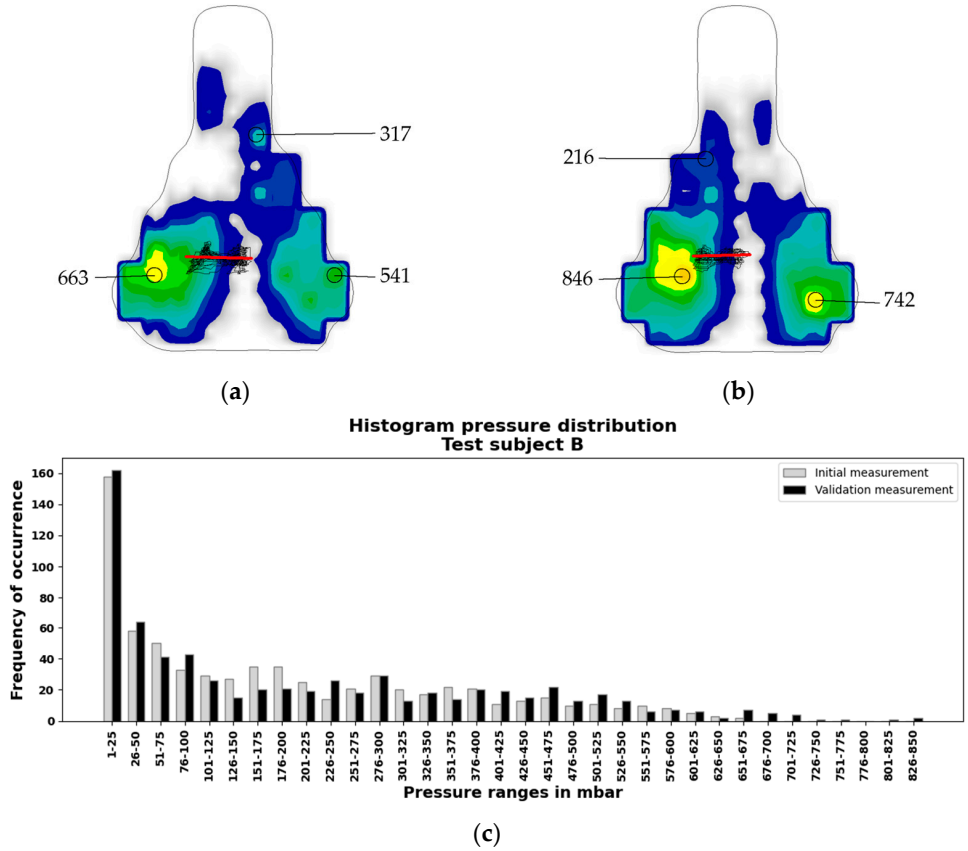

Figure 12. Visual representation of both measurements of test subject B; (**a**) color plot with peak pressure values of the initial measurement, (**b**) color plot with peak pressure values of the validation measurement—blue, low pressure to orange, high pressure, and (**c**) histogram of both measurements.

Figure 12b illustrates the pressure distribution of test subject B with the custom saddle pad. In contrast to the objective of reducing pressure peaks, the peak pressure on the right

side increased by 28% and on the right half of the saddle by 37%. However, the analysis of the measurement data indicates a markedly more uniform distribution across both saddle halves compared to the CFRP shell. Additionally, the pressure in the front area has shifted slightly towards the back. Despite this increase in peak pressure, the pressure distribution on the saddle has become more uniform overall.

The frequency distribution of pressure values between the initial and validation measurements is also largely analogous for test subject B (Figure 12c). In the initial area, the frequencies of the validation measurement exceed those of the initial measurement. Subsequently, a precipitous decline in the values is observed. It is notable that for the range between 126 and 225 mbar, a greater number of values was recorded in the initial measurement. From 401 mbar, the frequencies of the validation measurement are predominant, reaching values above 675 mbar for the first time, indicating an increase in the peak pressure in the validation measurement. In comparison to test subject A, test subject B also exhibits the highest value in the lowest pressure ranges (1–25 mbar). However, the difference between the two measurements is less pronounced for test subject B than for test subject A. In the pressure ranges from 26 to 100 mbar and 101 to 250 mbar, subject B demonstrates a more consistent distribution, whereas subject A exhibits a pronounced decline in frequency. Overall, in the medium and higher pressure ranges (above 250 mbar), test subject B displays a more uniform distribution between the two measurements in comparison to test subject A.

3.6.3. Test Subject C

The most favorable outcomes were observed in test subject C. The pressure pattern on the CFRP shell (Figure 13a) demonstrated a peak pressure of 880 mbar on the left half of the saddle, which is comparable to the outcomes observed in test subject A. The right half of the saddle exhibited a balanced pressure distribution and can be described as sufficient in terms of pressure distribution. In contrast, the pressure distribution for test subject C is already highly homogeneous. Figure 13b depicts the pressure distribution with the personalized saddle pad. The peak pressure on the left side was markedly reduced by 46%, while the left half of the saddle exhibited a slight peak pressure reduction of 3%. The pressure pattern of this saddle pad was evaluated by the bike fitting expert as nearly optimal and is therefore the pressure pattern with the most significant improvement in pressure distribution of all three test subjects.

The histogram for the pressure distribution of test subject C (Figure 13c) demonstrates notable discrepancies between the initial measurement and the validation measurement. In the lowest pressure range of 1 to 25 mbar, the initial measurement (gray) exhibits the highest frequency, which is even slightly higher than that of the validation measurement (black). This indicates that a greater number of values were recorded within this low range in the initial measurement. The frequency observed in this instance is comparable to that observed in test subject B, while test subject A displays a lower frequency. In the pressure ranges from 26 to 100 mbar, there is a notable decline in frequency, which remains consistent between the first and second measurements. The mean pressure values, ranging from 101 to 350 mbar, exhibit a tendency towards higher values for the validation measurement within this range. In the higher pressure ranges above 250 mbar, an initial increase in frequency, comparable to that observed in test subject A, is evident. However, this trend reverses at approximately 350 mbar, exhibiting a decline in frequency. In the extremely high pressure ranges exceeding 700 mbar, a nearly continuous decline in the frequencies of the validation measurement relative to the initial measurement is evident in test subject C. This indicates that the peak pressure is also diminished. In comparison to test subjects A and B, test subject C exhibits a distinctive distribution pattern. In the lowest pressure range, the initial measurement displays a higher

frequency, which is not observed in the other test subjects. In the medium pressure ranges (26–250 mbar), subject C exhibits a higher frequency in the validation measurement, similar to subject B but with a somewhat more uniform distribution. The most pronounced shift in pressure values is observed in test subject C, who exhibited a transition from high ranges (over 650 mbar) to medium ranges (200–350 mbar).

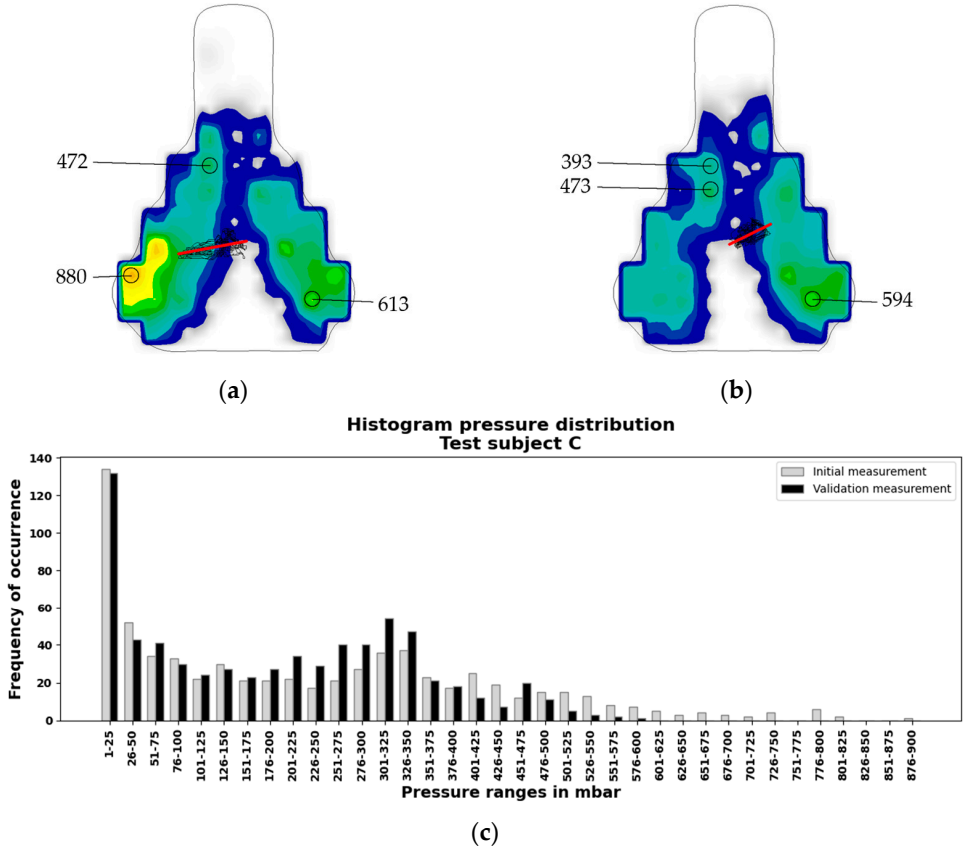

Figure 13. Visual representation of both measurements of test subject C; (**a**) color plot with peak pressure values of the initial measurement, (**b**) color plot with peak pressure values of the validation measurement—blue, low pressure to orange, high pressure, and (**c**) histogram of both measurements.

3.7. Final Assessment

In conclusion, the validation pressure measurements taken from the three test subjects riding the personalized saddle pads yielded several noteworthy findings. While test subjects A and C demonstrated varying degrees of pressure reduction, the peak pressure of test subject B exhibited a notable increase. Table 5 shows the alteration in peak pressure of the adapted saddle pad in comparison to the initial pressure measurement on the CFRP shell, organized according to the specific test subject. Subject A demonstrates a uniform reduction in peak pressure on both saddle halves, amounting to approximately 15%. Test subject B exhibited a notable elevation in peak pressure, approximating 30%, on both saddle halves. In contrast, test subject C demonstrated a peak pressure reduction of 46% on the left side and a modest enhancement of 4% on the right side.

The fifth row of the table presents the percentage change resulting from a comparison of the summed total pressure derived from the two measurements.

The individual values of the interpolated data set were aggregated to form a reference point for assessing the overall pressure on the saddle. If the position of the seat on the saddle remains constant, the value obtained from the two measurements should be identical, as the pressure cannot be reduced to zero. Should the total pressure differ between the two measurements, there may be a number of potential explanations for this discrepancy. For

example, the test subject may have experienced a change in body weight or the position of the body on the bicycle may have changed, which can result in an increase or decrease in the total pressure on the saddle. In this instance, the subjects' assessments diverge once more. In the case of test subject A, this effect has a beneficial impact on the overall pressure, which is reduced by 5%. However, as the peak pressure decreases by approximately 15% on both sides, it can be stated that an improved pressure distribution has been achieved for test subject A, which has been accomplished by the adapted saddle pad.

Table 5. Alteration in peak pressure.

Test Subject	A	B	C
Body size [cm]	184	180	185
Body weight [kg]	81	82	80
Accumulated pressure-Initial measurement [mbar]	142.440	129.730	159.450
Accumulated pressure-Validation measurement [mbar]	135.170	147.940	136.220
Pressure changes initial vs. validation [%]	−5.1	+14.01	−14.56
Peak pressure changes left [%]	−14.25	+27.6	−46.25
Peak pressure changes right [%]	−16.51	+37.15	−3.1

The assessment for test subject B shows an increase in both the peak pressures and the total pressure. Given the observed increase in total pressure by 14% and peak pressure by over 30%, it can be concluded that a change in sitting position or change in cadence during the validation measurement is an unlikely sole cause of the deterioration in pressure values. This leaves an error in measurement during the initial pressure measurement as the sole reasonable explanation. This is evidenced by the processed data in Figure 5b, which indicate that the pressure has been partially "lost" during the initial pressure measurement. In the case of test subject B, the validation measurement yielded a total pressure comparable to that observed in the other test subjects during the initial measurement conducted on the CFRP shell. Moreover, the modified saddle pad results in a more symmetrical pressure distribution despite the elevated pressures on the saddle, indicating that both halves of the saddle are now subjected to a nearly equal load. It would be beneficial to conduct a further pressure measurement of test subject B on the CFRP shell in order to eliminate the possibility of measurement errors in the initial measurement. Furthermore, a plausibility check must be incorporated into the overall process to safeguard against future measurement errors. This objective can be accomplished by first comparing all measurement results obtained from all test subjects to ascertain the pressure ranges. Subsequently, the data from each measurement, both from the initial and the validation measurements, should be processed and compared in accordance with the criteria outlined in Table 5.

Test subject C exhibited a balanced right half of the saddle without pressure peaks during the initial pressure measurement, which was maintained during the validation measurement. The total pressure change of −14% between the initial and validation measurements also had a beneficial impact on the overall result of the validation measurement. In essence, the outcome for subject C can be characterized as satisfactory. The pressure peak of the left saddle half was reduced by approximately 50%, while the already optimal right half was nevertheless slightly improved by −3%. It can thus be concluded that the considerable reduction in peak pressure for test subject C is attributable to the personalized saddle pad.

The findings indicated that the implementation of functionally graded lattice structures based on pressure measurement data can markedly enhance the pressure distribution on the bike saddle. This is particularly evident in the data collected from test subjects A and C. An increase in pressure values was observed in test subject B during the validation measurement, indicating that the initial pressure measurement of this test subject yielded incomplete or faulty data.

Long-term testing is a crucial component of evaluating the long-term efficacy and comfort of personalized saddles. The feedback from the test subjects was predominantly positive. Test subject A performed an alpine crossing, testing the saddle pad over a distance of 500 km and 3600 m of elevation gain. Test subject B completed approx. 280 km and 1700 m of elevation gain without any issues or failures of the lattice struts. In particular, test subject C completed over 1500 km with his customized saddle, with only one issue concerning the separation of glue in one isolated area.

4. Discussion

The integration of lattice structures into components is a complex process that necessitates the utilization of a modern computer system with sophisticated CAD software, in addition to advanced simulation and manufacturing techniques. This prompts the crucial question of whether and in what contexts it is appropriate to utilize lattice structures in designs that are inherently complex. It is crucial to recognize that the incorporation of lattice structures into components does not inherently address all challenges. Rather, there are specific applications in which they have been demonstrated to be a practical solution thus far and areas in which their use will prove advantageous in the near future, contingent on further research and the ongoing development of optimization possibilities.

Lattice structures have emerged as a prominent area of interest within the sports equipment industry, with applications spanning diverse product categories such as footwear (e.g., shoes) [42], head protection (e.g., helmets) [43], and bicycle components (e.g., saddles).

Figure 14 depicts a variety of bike saddles produced by different manufacturers. All of the aforementioned approaches utilize functionally graded lattice structures. However, it should be noted that all of the depicted structures were developed on the basis of extensive data obtained from athletes. The illustrated bike saddles and saddle pads were designed using Carbon®'s Design Engine Pro and manufactured using Carbon®'s own resin materials, in addition to the in-house Digital Light Synthesis™ (DLS) process.

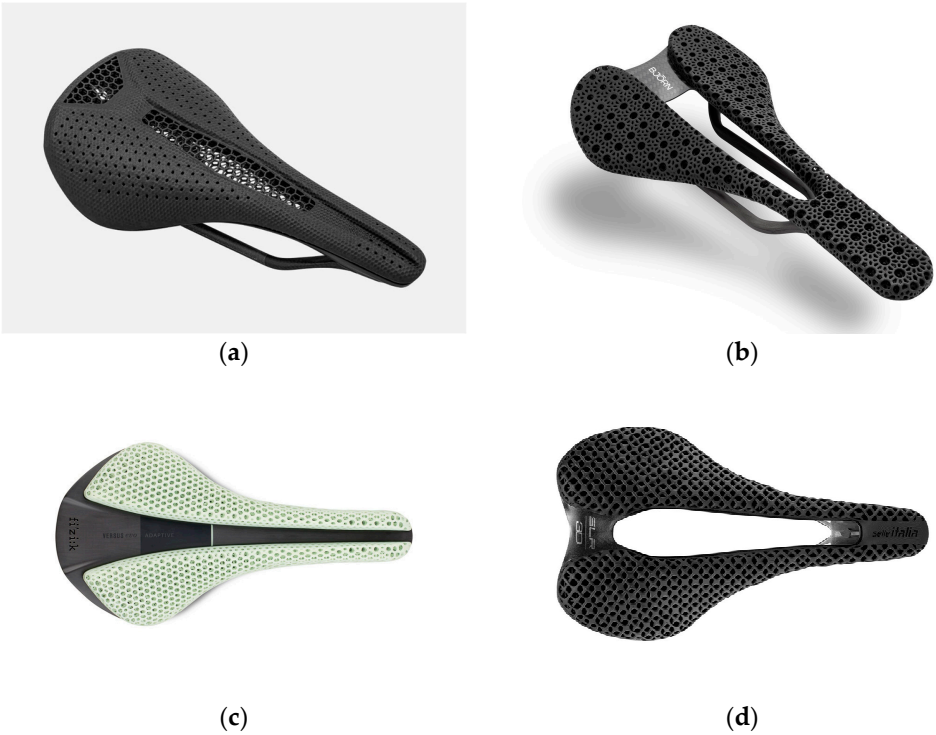

(**a**) (**b**)

(**c**) (**d**)

Figure 14. Different types of road bike saddles; (**a**) Specialized S-Works Phenom [44], (**b**) Björn Cycles Setka [45], (**c**) fizik Antares Verso Evo 00 Adaptive [46], (**d**) Selle Italia SLR Boost 3D [47].

It is also noteworthy to mention fizik ONE to ONE, as this company is pursuing a similar concept and offers valuable opportunities for comparison. The concept was first presented by Fizik during the preparation of this publication and is still relevant due to the similar approach. fizik ONE to ONE [48] is an individual fitting service that enables customers to receive personalized bike saddles. The process comprises the following steps:

1. Short "pressure fit": duration approx. 15 min (rough bike fitting).
2. First pressure measurement on your own bike with your own saddle (no statement about handlebar position).
3. Specific app (connected to pressure measuring system) suggests one of the three Fizik basic saddle shapes.
4. Second pressure measurement with suggested Fizik saddle shape.
5. An algorithm calculates the corresponding geometry required; six geometries are available in two saddle widths each, with the following strategy (derived from the image): high pressure, thicker struts; low pressure, thinner struts.
6. Saddle production (duration: approximately half a day).
7. Rails (selectable) are connected directly to the AM saddle structure.
8. Delivery time of assembled saddle: approximately two weeks.

In contrast, the methodology presented in this paper is as follows:

1. The data were collected through the use of pressure measurements. Subsequently, the participants underwent professional bike fitting, followed by the pressure measurement on the CFRP saddle shell. The objective was to record the pressure distribution and to focus on handlebar position 2, which is predominantly used when riding.
2. Analysis of the measurement data was performed. The pressure data were subjected to analysis and subsequently employed to modify the functionally graded lattice structure of the saddle. Each area can be modified independently and with high precision. The strategy employed was as follows: areas with pressure peaks would be softer than the adjacent hard areas, which then became constantly softer with lower pressure.
3. Modeling of personalized lattice structures: Carbon® Design Engine Pro software was employed to generate saddle pads that were tailored to the specified pressure distributions.
4. Production of the saddle pads: the saddle was manufactured using SLS and bonded to the existing CFRP saddle shell.
5. A second pressure measurement was conducted with the assistance of a professional bike fitter in order to provide a quantitative evaluation of the results.

The primary distinction between the two methodologies is in the method of data collection and fitting. While the fizik ONE to ONE performs a seat position analysis, the fitting in this study was based on the saddle pressure measurements, which were collected subsequent to comprehensive and professional bike fitting. Whilst both approaches are using the same pressure measurement system, the images of the Fizik saddle suggest that the company utilizes the raw measurement data rather than the interpolated data set (of higher resolution) that is also available from the measuring system and employed in this study (see Section 3.3). Design Engine Pro, provided by Carbon®, offers the unrestricted possibility of strut customization. This suggests that there are no software-related constraints with regard to lattice design and the highest possible resolution of sensor values for the generation of the functionally graded lattice. Moreover, Fizik does not provide a quantitative statement regarding the potential peak pressure reductions as well as improved pressure distribution that could be achieved with their technology.

While both approaches aim to optimize comfort and pressure distribution, further tests are required to develop a strategy that would demonstrably improve seating comfort

on the bike saddle pad developed in this study and on Fizik's saddles for a significant proportion of the population.

5. Conclusions

The objective of this project was to investigate and apply lattice structures in AM for the development of a personalized bike saddle pad. The potential of suitable strut-based gradient lattice structures based on the Voronoi formulation was evaluated and tested through this practical application using Carbon® Design Engine Pro software. The saddle pads were developed and individually adapted based on the pressure distribution and specific requirements of chosen test subjects. The selection of both AM processes and corresponding materials, as well as the compression testing of test samples and the modeling of prototypes and their subsequent production, were described in detail. Initial pressure measurements were conducted with three test subjects of similar body mass and height in order to evaluate and optimize the individually adapted saddle pads.

The initial pressure measurements, which included bike fitting procedures, were conducted in varying cycles between three and six cycles, contingent upon the experience level of each rider. The measurements were conducted in the sitting position that was deemed most comfortable by the bike fitter based on pressure mapping and the test subject based on personal perception. Subsequently, a single peak pressure measurement was selected for each test subject and defined as baseline for the subsequent pad design phase.

The design of the bespoke saddle pads was achieved through the utilization of Carbon's® Design Engine Pro, employing Voronoi-based functionally graded lattice structures. The three saddle pads were produced through the application of SLS, utilizing TPU material, and they were subsequently bonded to CFRP saddle shells.

Validation measurements were conducted to ascertain whether the use of the saddle pads would result in a notable improvement in comfort for the three test subjects.

The results demonstrate that the implementation of structural innovations, such as the utilization of gradient Voronoi lattice structures, has the capacity to enhance performance by reducing pressure peaks and facilitating the uniform distribution of pressure across the saddle. The bespoke designs are tailored to the specific anatomical characteristics of the rider, thereby enhancing both comfort and stability. While pressure distribution values were enhanced in all three test subjects, peak pressure values could only be reduced in test subjects A and C. An increase in peak pressure values was observed in test subject B during the second measurement; the cause of this was determined to be incomplete and faulty data from the initial pressure measurement. Additional measures such as plausibility checks and the additional processing and comparison of the measurement data to ensure the validity of the measured pressure data sets were proposed.

All three test subjects participated in extended test rides, and the results were overwhelmingly positive. The riders reported enhanced riding comfort and a reduction in discomfort, including soreness and muscle fatigue. Additionally, there was a notable decrease in pressure on the pelvic floor muscles.

Author Contributions: Conceptualization, S.G., J.S. and C.H.; methodology, S.G. and J.S.; investigation, S.G. and J.S.; data curation, S.G., J.S. and C.H.; writing, S.G. and J.S.; visualization, S.G. and J.S.; supervision, C.H. All authors have read and agreed to the published version of the manuscript.

Funding: The research leading to these results was partly funded under the cooperative doctoral program "Digiphot" between FH Campus Wien and TU Wien. Open Access funding by TU Wien.

Institutional Review Board Statement: Not applicable.

Informed Consent Statement: Informed consent was obtained from all subjects involved in the study.

Data Availability Statement: The raw data supporting the conclusions of this article will be made available by the authors upon request.

Acknowledgments: We would like to extend our gratitude to Veletage GmbH, in particular, Kurt Stefan and Joshua M. Hayes, for their invaluable assistance. This has included professional bike fitting, the provision of a measuring system, and numerous hours of professional discourse, offering detailed insight into the intricacies of the professional bicycle industry. We would like to extend our gratitude to Bjorn d.o.o. for the provision of CFRP saddle shells at no cost and for offering their expert opinion on the most suitable bonding agents. We would like to express our gratitude to SnM gebioMized GmbH for their invaluable online assistance with the Saddle Mapping Pressure Tool. We would like to express our gratitude to David Nechi for his assistance with the manufacturing and post-processing of the SLS parts, which were built by our EOS Formiga P110. We would like to express our gratitude to Christian Halter for the 3D scanning of the original CFRP saddle shell. We would also like to thank Carbon® for the extended trial period of their Design Engine Pro software and their professional support. Furthermore, I would like to thank Jürgen Stampfl for his supervision of this work and for his supervision of my dissertation at TU Wien. The authors acknowledge TU Wien Bibliothek for financial support and Open Access Funding by TU Wien.

Conflicts of Interest: The authors declare no conflicts of interest. Although Carbon® provided the software Design Engine Pro free of charge for an extended period of time, the company had no role in the design of the study; in the collection, analyses, or interpretation of data; in the writing of the manuscript; or in the decision to publish the results.

References

1. Attaran, M. The rise of 3-D printing: The advantages of additive manufacturing over traditional manufacturing. *Bus. Horiz.* **2017**, *60*, 677–688. [CrossRef]
2. Ford, S.; Despeisse, M. Additive manufacturing and sustainability: An exploratory study of the advantages and challenges. *J. Clean. Prod.* **2016**, *137*, 1573–1587. [CrossRef]
3. Raut, L.P.; Taiwade, R.V. Wire Arc Additive Manufacturing: A Comprehensive Review and Research Directions. *J. Mater. Eng. Perform.* **2021**, *30*, 4768–4791. [CrossRef]
4. Steenhuis, H.-J.; Pretorius, L. The additive manufacturing innovation: A range of implications. *J. Manuf. Technol. Manag.* **2017**, *28*, 122–143. [CrossRef]
5. Jiang, R.; Kleer, R.; Piller, F.T. Predicting the future of additive manufacturing: A Delphi study on economic and societal implications of 3D printing for 2030. *Technol. Forecast. Soc. Change* **2017**, *117*, 84–97. [CrossRef]
6. Matos, F.; Godina, R.; Jacinto, C.; Carvalho, H.; Ribeiro, I.; Peças, P. Additive Manufacturing: Exploring the Social Changes and Impacts. *Sustainability* **2019**, *11*, 3757. [CrossRef]
7. Caviggioli, F.; Ughetto, E. A bibliometric analysis of the research dealing with the impact of additive manufacturing on industry, business and society. *Int. J. Prod. Econ.* **2019**, *208*, 254–268. [CrossRef]
8. Huang, S.H.; Liu, P.; Mokasdar, A.; Hou, L. Additive manufacturing and its societal impact: A literature review. *Int. J. Adv. Manuf. Technol.* **2013**, *67*, 1191–1203. [CrossRef]
9. Wohlers Associates (Ed.) *Wohlers Report 2023: 3D Printing and Additive Manufacturing Global State of the Industry*; Wohlers Associates: Washington, DC, USA, 2023; ISBN 978-1-62204-966-0.
10. Boschetto, A.; Bottini, L.; Macera, L.; Vatanparast, S. Additive Manufacturing for Lightweighting Satellite Platform. *Appl. Sci.* **2023**, *13*, 2809. [CrossRef]
11. Arena, M.; Ambrogiani, P.; Raiola, V.; Bocchetto, F.; Tirelli, T.; Castaldo, M. Design and Qualification of an Additively Manufactured Manifold for Aircraft Landing Gears Applications. *Aerospace* **2023**, *10*, 69. [CrossRef]
12. nTopology, Inc. nTop. Available online: https://www.ntop.com/ (accessed on 1 April 2024).
13. Altair Engineering Inc. Sulis. Available online: https://www.altair.com/sulis (accessed on 1 April 2024).
14. Altair Engineering Inc. Inspire. Available online: https://altair.com/inspire (accessed on 1 April 2024).
15. Carbon Inc. Design Engine Pro. Available online: https://www.carbon3d.com/products/carbon-design-engine (accessed on 1 April 2024).
16. Autodesk Netfabb Ultimate. Available online: https://www.autodesk.com/de/products/netfabb/overview?plc=F360NFP&term=1-YEAR&support=ADVANCED&quantity=1&tab=subscription (accessed on 28 October 2024).
17. Metafold 3D. Metafold. Available online: https://www.metafold3d.com/ (accessed on 26 September 2024).

18. Gibson, L.J. Cellular Solids. *MRS Bull.* **2003**, *28*, 270–274. [CrossRef]
19. Pan, C.; Han, Y.; Lu, J. Design and Optimization of Lattice Structures: A Review. *Appl. Sci.* **2020**, *10*, 6374. [CrossRef]
20. Gibson, L.J. Modelling the mechanical behavior of cellular materials. *Mater. Sci. Eng. A* **1989**, *110*, 1–36. [CrossRef]
21. Gibson, L.J.; Ashby, M.F. *Cellular Solids: Structure and Properties*, 2nd ed.; Cambridge University Press: Cambridge, UK, 1997; ISBN 978-0-521-49911-8.
22. Georges, H.; García Solera, D.; Aguilar Borasteros, C.; Metar, M.; Song, G.; Mandava, R.; Becker, W.; Mittelstedt, C. Mechanical Performance Comparison of Sandwich Panels with Graded Lattice and Honeycomb Cores. *Biomimetics* **2024**, *9*, 96. [CrossRef] [PubMed]
23. Chen, W.; Chen, C.; Zhang, Y.; Li, P.; Li, M.; Li, X. Study on the Deformation Mode and Energy Absorption Characteristics of Protective Honeycomb Sandwich Structures Based on the Combined Design of Lotus Root Nodes and Leaf Stem Veins. *J. Mar. Sci. Eng.* **2024**, *12*, 652. [CrossRef]
24. Mott. Available online: https://mottcorp.com/blog/mott-presents-cutting-edge-technology-in-additive-manufacturing-at-the-international-conference-on-sintering-2017/ (accessed on 17 April 2024).
25. Alknery, Z.; Sktani, Z.D.I.; Arab, A. Effect of Cell Geometry on the Mechanical Properties of 3D Voronoi Tessellation. *J. Funct. Biomater.* **2022**, *13*, 302. [CrossRef] [PubMed]
26. Kedziora, S.; Decker, T.; Museyibov, E. Application of Functionally Graded Shell Lattice as Infill in Additive Manufacturing. *Materials* **2023**, *16*, 4401. [CrossRef]
27. Song, R.; Moorehead, M.; Yushu, D.; Ke, J.-H. Lattice Design and Advanced Modeling to Guide the Design of High-Performance Lightweight Structural Materials. *Energies* **2024**, *17*, 1468. [CrossRef]
28. Dong, G.; Tessier, D.; Zhao, Y.F. Design of Shoe Soles Using Lattice Structures Fabricated by Additive Manufacturing. *Proc. Des. Soc. Int. Conf. Eng. Des.* **2019**, *1*, 719–728. [CrossRef]
29. Zhang, C.; Chen, F.; Huang, Z.; Jia, M.; Chen, G.; Ye, Y.; Lin, Y.; Liu, W.; Chen, B.; Shen, Q.; et al. Additive manufacturing of functionally graded materials: A review. *Mater. Sci. Eng. A* **2019**, *764*, 138209. [CrossRef]
30. Yang, L.; Mertens, R.; Ferrucci, M.; Yan, C.; Shi, Y.; Yang, S. Continuous graded Gyroid cellular structures fabricated by selective laser melting: Design, manufacturing and mechanical properties. *Mater. Des.* **2019**, *162*, 394–404. [CrossRef]
31. Després, N.; Cyr, E.; Setoodeh, P.; Mohammadi, M. Evolutionary computation to design additively manufactured optimal heterogeneous lattice structures. *Prog. Addit. Manuf.* **2023**, *8*, 615–627. [CrossRef]
32. Geyer, S.; Hölzl, C. Comparison of CAD Software for Designing Cellular Structures for Additive Manufacturing. *Appl. Sci.* **2024**, *14*, 3306. [CrossRef]
33. EOS GmbH. MDS EOS TPU 1301. Available online: https://www.eos.info/en-us/polymer-solutions/polymer-materials/data-sheets/mds-eos-tpu-1301 (accessed on 27 September 2024).
34. Cubicure GmbH. Evonik INFINAM® FL 6300 L Powered by Cubicure. Available online: https://cubicure.com/3d-anlagen-materialien-produktuebersicht/materialien/infinam/ (accessed on 27 September 2024).
35. Cubicure GmbH. Caligma. Available online: https://cubicure.com/caligma/ (accessed on 27 September 2024).
36. Cubicure GmbH. Hot Lithography. Available online: https://cubicure.com/en/hot-lithography/ (accessed on 27 September 2024).
37. *ISO 604:2002(E)*; Plastics—Determination of Compressive Properties. Austrian Standards International: Wien, Austria, 2024.
38. Schwemmer, J. Creating lattice structures with the programs Autodesk Netfabb and Carbon Design Engine Pro. Master's Thesis, University of Applied Sciences FH Campus Wien, Wien, Austria, 2024. 118.
39. Velotraum. Fahrradanpassung, Bikefitting. Available online: https://velotraum.de/system/anpassung/ (accessed on 9 September 2024).
40. Carbon. Specialized Innovates at 2x the Speed with Carbon. Available online: https://www.carbon3d.com/resources/innovation-at-2x-the-speed (accessed on 24 September 2024).
41. Bjorn. Bjorn Cycles: Composite Saddles, Seatposts, Handlebars, etc. Available online: https://bjorncycles.com (accessed on 24 September 2024).
42. Carbon Inc. Whitepaper, Adidas. Available online: https://www.carbon3d.com/resources/whitepaper/the-adidas-story (accessed on 19 April 2024).
43. Decker, T.; Kedziora, S. Optimizing the Thickness of Functionally Graded Lattice Structures for High-Performance Energy Absorption: A Case Study Based on a Bicycle Helmet. *Appl. Sci.* **2024**, *14*, 2788. [CrossRef]
44. Specialized, S-Works Phenom mit Mirror. Available online: https://www.specialized.com/at/de/s-works-phenom-mit-mirror/p/1000148879?color=1000148881-1000148879 (accessed on 19 April 2024).
45. Bjorn. Bjorn Cycles, Setka. Available online: https://bjorncycles.com/tproduct/135716637-242246431431-setka (accessed on 19 April 2024).
46. Fizik, Antares Versus Evo 00 Adaptive. Available online: https://www.fizik.com/de_de/antares-versus-evo-00-adaptive.html (accessed on 19 April 2024).

47. Selle Italia, SLR Boost 3D Kit Carbonio Superflow. Available online: https://de.selleitalia.com/slr-boost-3d-kit-carbonio-superflow/ (accessed on 19 April 2024).
48. Fizik. Fizik ONE to ONE. 2024. Available online: https://www.fizik.com/eu_en/one-to-one (accessed on 25 October 2024).